THE JOURNAL OF BIOLOGICAL CHEMISTRY VOL. 283, NO. 32, pp. 22283–22294, August 8, 2008

Protein Kinase C Modulates Inactivation of Kv3.3 Channels*

Received for publication, February 29, 2008, and in revised form, June 4, 2008 Published, JBC Papers in Press, June 6, 2008, DOI 10.1074/jbc.M801663200

Rooma Desai[‡§], Jack Kronengold[‡], Jianfeng Mei[‡], Stuart A. Forman[§], and Leonard K. Kaczmarek[‡¶1]

From the [‡]Departments of Pharmacology and [¶]Cellular and Molecular Physiology, Yale School of Medicine, New Haven, Connecticut 06520 and the [§]Department of Anesthesia and Critical Care, Massachusetts General Hospital, Boston, Massachusetts 02114

Modulation of some Kv3 family potassium channels by protein kinase C (PKC) regulates their amplitude and kinetics and adjusts firing patterns of auditory neurons in response to stimulation. Nevertheless, little is known about the modulation of Kv3.3, a channel that is widely expressed throughout the nervous system and is the dominant Kv3 family member in auditory brainstem. We have cloned the cDNA for the Kv3.3 channel from mouse brain and have expressed it in a mammalian cell line and in *Xenopus* oocytes to characterize its biophysical properties and modulation by PKC. Kv3.3 currents activate at positive voltages and undergo inactivation with time constants of 150–250 ms. Activators of PKC increased current amplitude and removed inactivation of Kv3.3 currents, and a specific PKC pseudosubstrate inhibitor peptide prevented the effects of the activators. Elimination of the first 78 amino acids of the N terminus of Kv3.3 produced noninactivating currents suggesting that PKC modulates N-type inactivation, potentially by phosphorylation of sites in this region. To identify potential phosphorylation sites, we investigated the response of channels in which serines in this N-terminal domain were subjected to mutagenesis. Our results suggest that serines at positions 3 and 9 are potential PKC phosphorylation sites. Computer simulations of model neurons suggest that phosphorylation of Kv3.3 by PKC may allow neurons to maintain action potential height during stimulation at high frequencies, and may therefore contribute to stimulus-induced changes in the intrinsic excitability of neurons such as those of the auditory brainstem.

Kv3 family voltage-dependent potassium channels have fast activation and deactivation kinetics and high activation thresholds, allowing many neurons that express these channels to fire trains of action potentials at high frequencies (1–4). Such rapid firing is, for example, essential for the ability of many auditory brainstem neurons to lock their action potentials to the phase of auditory inputs at firing rates of up to ~800 Hz (5–10).

Phosphorylation of potassium channel proteins is a regulatory mechanism by which membrane excitability is modulated downstream of the action of neurotransmitters and other stimuli (2, 11). Of the four channels in the Kv3 family (Kv3.1–Kv3.4) (1, 12), three (Kv3.1, Kv3.2, and Kv3.4) have been shown to be potently modulated by protein kinases. The Kv3.1 channel is regulated by both protein kinase C (PKC)[2] and casein kinase 2 (13, 14). Phosphorylation by PKC of a serine in the C terminus of Kv3.1b produces a decrease in current amplitude (14). Changes in the phosphorylation of this site within neurons of the medial nucleus of the trapezoid body (MNTB) are produced by changes in the auditory environment, and this regulates the ability of the neurons to fire at high rates with temporal accuracy (2). Phosphorylation of Kv3.4 channels by PKC prevents their inactivation during depolarizing commands (15), whereas phosphorylation of Kv3.2 channels by protein kinase A decreases current amplitudes (16).

In contrast to the above channels, relatively little is known about the modulation of Kv3.3 currents by protein kinases. Kv3.3 is widely expressed in the nervous system and is the dominant Kv3 family member in the auditory brainstem (17). For example, Kv3.3 protein is expressed in the calyces of Held, the large presynaptic terminals that provide input to the MNTB, and also in the superior olivary complex, where the axons of MNTB neurons terminate (17, 18). Although these neurons and terminals have served as a model system of the investigation of the roles and modulation of potassium channels in control of firing patterns, the role of Kv3.3 channels in the physiology of these auditory pathways remains unknown.

In this study, we have characterized the electrophysiological properties of mouse Kv3.3 channels in recombinant systems and found that Kv3.3 currents are potently enhanced by activation of PKC. We have identified two N-terminal serine residues that are consensus sites for PKC phosphorylation and that are required for enhancement of Kv3.3 currents. We have also carried out numerical simulations to assess the potential effects of this modulation on firing patterns in a model of MNTB neurons. Our results show that PKC modulation of Kv3.3 channels could play a role in dynamic adaptation of auditory brainstem circuits.

EXPERIMENTAL PROCEDURES

Cloning of Kv3.3 cDNA from Mouse Brainstem—Total RNA was isolated from whole brain of two 16-day-old SvJ129 mice using the Ultraspec-II RNA kit (Biotecx Laboratories Inc., Houston, TX). The messenger RNA was isolated from the total RNA using the Oligotex kit (Qiagen, Valencia, CA). For cloning the 5′-end of the gene, 5′-rapid amplification of cDNA ends (RACE) strategy (19)

* This work was supported, in whole or in part, by National Institutes of Health Grant DC-01919 (to L. K. K.). The costs of publication of this article were defrayed in part by the payment of page charges. This article must therefore be hereby marked "*advertisement*" in accordance with 18 U.S.C. Section 1734 solely to indicate this fact.

[1] To whom correspondence should be addressed: Dept. of Pharmacology, Yale School of Medicine, 333 Cedar St., New Haven, CT 06520. Tel.: 203-785-4500; Fax: 203-785-5494; E-mail: leonard.kaczmarek@yale.edu.

[2] The abbreviations used are: PKC, protein kinase C; CHO, Chinese hamster ovary; MNTB, medial nucleus of the trapezoid body; PBS, phosphate-buffered saline; RACE, rapid amplification of cDNA ends; μS, microsiemens.

was used. Briefly, mRNA was primed with the gene-specific primer 5′-CGGTCGAAGAAGAACTCG-3′ based on the previously reported mouse Kv3.3 nucleotide sequence (GenBank™ accession number S69381) (20, 21). Single-stranded cDNA was synthesized from 250 ng of poly(A^+) RNA using 200 units of Superscript II™ RNase H^- reverse transcriptase (Invitrogen). The resulting cDNA was cleaned using Microcon-100 (Millipore, Billerica, MA) filters. Terminal deoxynucleotidyltransferase enzyme (Invitrogen) was used to add a poly(A^+) tail on the 5′-end of the first-strand cDNA. This single-stranded cDNA was then used as a template for the first round of PCR using the following primers: Q_T (5′-CCAGTGAGCAGAGTGACGAGGACTCGAGCTCAAGCTTTTTTTTTTTTTTTT-3′), Q_{out} (5′-CCAGTGAGCAGAGTGACG-3′), and Kv3.3-specific primer 5′-GGGTCGTAGTCAAAGCGC-3′. The resulting PCR was diluted and used for a second nested PCR using the primers Q_{in} (5′-GAGGACTCGAGCTCAAGC-3′) and Kv3.3-specific primer 5′-GGCAGGGTGCGCAACGTG-3′. A PCR product of about 370 bp was obtained and was subcloned into a plasmid for automated DNA sequencing. All PCRs were performed using the proofreading *Pfu* DNA polymerase (Stratagene, La Jolla, CA), and the PCR products were A^+-tailed using *Taq* polymerase (Qiagen, Valencia, CA) before subcloning in pCR2.1-TOPO plasmid (Invitrogen). The sequence obtained lacked the first two amino acids of a previously reported protein sequence (GenBank™ accession number Q63959). We used this sequence to search similar expressed tagged sequences in the GenBank™. A 606-bp mouse expressed sequence tags (GenBank™ accession number BE949391) was found, which further extended our sequence in the 5′-region by 230 bp. A PCR with primers 5′-CTGAGCTTTCTGTGCAACC-3′ and 5′-GGCAGGGTGCGCAACGTG-3′ on the previously prepared single-stranded cDNA confirmed the co-linearity of the overlapping cDNA fragments.

The remaining 3′-terminal cDNA sequence was also cloned using a 3′-RACE-PCR strategy and was identical to the previously reported mouse Kv3.3 sequence (GenBank™ accession number Q63959) (21). The full-length cDNA containing the 5′- and 3′-untranslated region was pieced together with several subcloning steps using restriction enzymes and was finally subcloned into pCDNA3 plasmid (Invitrogen) for expression into mammalian cells and *Xenopus* oocytes. Sequences were aligned using on-line multiple sequence alignment software (22).

Cell Culture and Preparation of Stable Cell Line Expressing Kv3.3 Channel—Chinese hamster ovary (CHO) cells were grown in Iscove's modified Dulbecco's medium (Invitrogen) supplemented with 10% fetal bovine serum (heat-inactivated), 100 units/ml penicillin/streptomycin, 0.1 mM hypoxanthine, and 0.01 mM thymidine in a 5% CO_2 incubator at 37 °C. For preparing stable cell line, cells were seeded 1 day before transfection. Lipofectamine (Invitrogen) was used to transfect CHO cells with Kv3.3 expression vector (pCDNA3) 24 h later. The cells were then grown in normal media for 48 h to develop antibiotic resistance and were subsequently exposed to geneticin (0. 5 mg/ml, Invitrogen) for another 2 weeks. The geneticin-resistant cells were subjected to single-cell sorting using FACSIV (BD Biosciences) to generate individual stable cell lines.

Membrane Isolation and Western Blotting—Whole mouse brain (15 days; SvJ129 mice) were dissected out in ice-cold phosphate-buffered saline (PBS) and suspended in cold homogenization buffer (50 mM Tris-HCl, pH 7.4, 1 mM EDTA, and Complete Mini Protease Inhibitor Tablet (Roche Applied Science)). Cultured CHO cells were harvested and washed twice in cold PBS and were then resuspended in cold homogenization buffer. Cultured cells and whole brains were then homogenized with a Teflon glass homogenizer, and the homogenate was centrifuged at 1,000 × *g* for 5 min (at 4 °C) to remove large cell debris. The supernatant was centrifuged at 21,000 × *g* for 30 min (at 4 °C), and the membrane pellet (crude membrane fraction) was resuspended in cold homogenization buffer and sonicated for 30 s. The membrane homogenates were then aliquoted, quickly frozen in liquid nitrogen, and stored at −70 °C until use. Protein estimation was done using Bradford's reagent (Bio-Rad). 30 μg of protein of each sample was loaded in each lane. Samples were suspended in 1× sample buffer (62.5 mM Tris, pH 6.8, 4% SDS, 10% glycerol, 0.02% bromphenol blue, and 4% β-mercaptoethanol) and warmed at 45 °C for 5 min and cooled on ice for 10 min before loading on a 4–15% linear gradient Tris-HCl gel (Bio-Rad) for electrophoresis. After electrophoresis, the protein was transferred onto an activated polyvinylidene difluoride membrane (Bio-Rad) at 100 V for 1 h in a chilled transfer buffer (25 mM Tris, 192 mM glycine, and 10% methanol) at 4 °C. Efficiency of transfer was checked with Ponceau stain (Bio-Rad). Blots were air-dried overnight and then blocked in PBS containing 10% nonfat milk and 0.05% Tween 20 (blocking buffer) for 1 h at room temperature with shaking. Blots were then incubated with the respective primary antibody overnight at 4 °C. After three washes with blocking buffer, blots were incubated for 1 h with horseradish peroxidase-conjugated secondary antibody, followed by extensive washes in PBS. Labeled proteins were detected by enhanced chemiluminescence. Blots were stripped with 0.2 M NaOH for 5 min at room temperature. Polyclonal anti-rat Kv3.3 antibodies (Alomone Labs, Jerusalem, Israel) were used at 5 μg/ml. The monoclonal anti-Na^+/K^+-ATPase α-1 (Millipore, Billerica, MA) was used at 0.1 μg/ml.

Patch Clamp Recordings from CHO Cells—Stable cell line of CHO cells expressing Kv3.3 channels were seeded on polylysine (Sigma)-coated glass coverslips (Bellco Biotechnology, Vineland, NJ) 24 h prior to recordings in growth condition described above. Recordings were made with Axopatch 2D amplifier (Molecular Devices, Sunnyvale, CA). The patch electrodes were pulled from 1.5-mm OD borosilicate capillary glass (World Precision Instruments, Sarasota, FL) using a puller (Sutter Instruments, Novato, CA). The resistance of a typical electrode was 1.5–2 megohms for whole-cell recording and 7–10 megohms for single channel recordings when filled with intracellular solution. For whole-cell recordings, the intracellular solution consisted of (in mM) 97.5 potassium gluconate, 32.5 KCl, 10 HEPES, 5 EGTA, and 1 $MgCl_2$, pH 7.3, with KOH. The bath solution consisted of (in mM) 145 NaCl, 5 KCl, 1 $MgCL_2$, 2 $CaCl_2$, 10 HEPES, 10 glucose, pH 7.3, with NaOH. Series resistance was less then 5 megohms and was compensated by 80–85% with a lag of 10 μS. The capacitance of CHO cells ranged from 9 to 13 picofarads. The data were acquired at 10

kHz and filtered at 5 kHz. Data were leak subtracted on line with p/4. For cell-attached single channel recordings, bath solution consisted of (in mM) 175 KCl, 4 $MgCl_2$, and 10 HEPES (pH 7.3 titrated with KOH). The pipette solution consisted of (in mM) 145 NaCl, 5 KCl, 1 $MgCl_2$, 2 $CaCl_2$, 10 HEPES, and 10 glucose (pH 7.2 titrated with NaOH). The single channel data were acquired at 10 kHz and filtered on line at 5 kHz. For analysis and presentation, the data were further filtered in Clampfit 9 (Molecular Devices, Sunnyvale, CA) using the digital Gaussian filter at 500 Hz. Capacitive transients were blanked for data presentation. Data were acquired using pClamp8 software (Molecular Devices, Sunnyvale, CA).

Electrophysiological Recordings from Xenopus Oocytes—Linearized mouse Kv3.3 cDNA in mammalian expression plasmid pCDNA3 was used as a template to produce capped mRNA by *in vitro* transcription driven by T7 RNA polymerase (mMESSAGE mMACHINE, Ambion, Austin, TX). Harvesting of the oocyte and microinjection was done by standard procedures (23). Injected oocytes were incubated at 18 °C for 1–7 days before electrophysiological recordings. Data acquisition was done using pClamp8 software (Molecular Devices, Sunnyvale, CA). Two-electrode voltage clamp recordings from *Xenopus* oocytes were carried out at 21–23 °C using a OC-725C oocyte clamp amplifier (Warner Instruments, Hamden, CT) and were carried out in ND-96 as bath solution (in mM) as follows: 96 NaCl, 2 KCl, 1.8 $CaCl_2$, 1 $MgCl_2$, and 5 HEPES (pH 7.4; titrated with NaOH). Whole-oocyte currents were digitized at 10 kHz and low pass filtered at 1 kHz. Currents were evoked by applying 1000-ms voltage steps from a holding potential of −80 to +70 mV in 10-mV increments. No leak subtractions were done. The typical oocyte leaks were 0.02–0.06 μA throughout the recordings except when cell-permeable Pseudo-Rack1 was applied. In the presence of Pseudo-Rack the leak increased up to 0.3 μA for some cells. The capacitive transients were blanked for data presentation. Stock solutions of Bryostatin1 (Tocris, Ellisville, MO) were dissolved in DMSO, aliquoted, and stored at −20 °C. Stock solution of Pseudo-Rack1 (Tocris, Ellisville, MO) and PKC pseudosubstrate-(19–31) (Tocris) were prepared by dissolving the peptides in ND-96 and also stored at −20 °C. Working dilutions in ND-96 were prepared right before use.

Data Analysis—To calculate conductance-voltage relations, currents were evoked by applying 800-ms voltage steps from a holding potential of −70 mV to potentials up to +70 mV in 10-mV increments. Conductance (G) values were obtained using the equation $G = I_K/(V - E_K)$, using the calculated value of −82 mV for E_K, and were then normalized to the maximum conductance (G_{max}). To determine steady-state inactivation, cells were held at −75 mV before giving a 730-ms pre-pulse to potentials between −100 and +50 mV in 10-mV increments, followed by a 250-ms test pulse to +20 mV. Both conductance and steady-state inactivation curves were fit using Boltzmann sigmoidal equation. To measure rates of deactivation, currents were activated by stepping from −70 mV to +50 mV for 5 ms and then stepping to potentials between −110 and 40 mV in 10-mV increments for 10 ms. Time constants (τ) of activation, inactivation, and deactivation were obtained by fitting current traces with a single term exponential equation on the rising, inactivating, and deactivating phases of current traces. The time course of recovery from inactivation was determined by first inactivating the currents by stepping from −100 to 20 mV for 2000 ms. This was followed by a step to −100 mV for varying durations that increased in increments of 7.5 or 100 ms, after which a test pulse was given (+ 40 mV for 350 ms). Normalized amplitudes (I) to maximum (I_{max}) values at 40 mV were plotted against the inter-pulse interval and fitted with a single exponential decay equation.

Because treatment of Kv3.3-expressing cells with activators of PKC typically result in near total loss of inactivation during depolarizing pulses lasting 1 s, it was not possible to determine accurate time constants for inactivation under these conditions. To quantify the loss of inactivation, we therefore scaled the peak currents before and after drug treatment and then determined the percentage increase in current at the end of a 1-s depolarizing command.

All electrophysiological data were analyzed using Clampfit 9 software (Molecular Devices, Sunnyvale, CA), and statistical analysis and curve fittings were done using GraphPad Prism 4 (GraphPad Software Inc., San Diego, CA) unless noted otherwise. For single channel data, the values for NP_o (where NP_o indicates number of channels × probability of opening) and amplitude were obtained by using the event statistics algorithms of Clampfit 9. The NP_o values were normalized by the total number of current levels open at positive potentials. For amplitude histograms, the amplitude data for level one were extracted from the event lists generated by the single channel search using the fast graph option. A conventional histogram was plotted with a bin width of 0.1 pA, and the histogram was fitted with the Gaussian equation using the Levenberg-Marquardt algorithm, and the number of terms was determined by comparing models. For data presentation, the histogram plots for single channel analysis were plotted using Origin 6 (Originlab Corp., Northampton, MA). For all experiments, statistical analysis was carried out using paired Student's t tests. A minimum p value of <0.05 was selected to determine significance. Averaged data are expressed as means ± S.E.

Site-directed Mutagenesis—Point and deletion mutations in Kv3.3 channel cDNA were introduced by full-length PCR amplification of plasmid DNA with sense and antisense mutated primers using *Pfu* polymerase (Stratagene, La Jolla, CA). Parental (wild type) DNA was digested with DpnI (New England Biolabs, Ipswich, MA), and 1 μl of this reaction was used for transformation of competent *Escherichia coli* XL1Blue strain (Stratagene, La Jolla, CA). Miniprep DNA was used for sequencing to confirm the presence of the desired mutation. The whole Kv3.3 cDNA was sequenced to verify no other undesired mutations were introduced during PCR. In total, 13 mutants were made: Δ78 (lacking the first 78 amino acids) and S3A, S4A, S9A, S32A, S33A, S46A, S53A, S60A, S3T, S3C, S3D, and S9D.

Numerical Simulations—Simulations of a hypothetical rapidly firing neurons were based on a previously described model of MNTB neurons (2, 3, 14, 24, 25) except that kinetic parameters for the Kv3.1 channel in this model were replaced by those matching Kv3.3. Responses were simulated by integration of the equation $-C\,dV/dt = I_{Na} + I_{Kv3.3} + I_{KvLT} + I_L + I_{ext(t)}$,

```
                1        10        20        30        40        50        60        70        80        90       100
                |--------+---------+---------+---------+---------+---------+---------+---------+---------+---------|
murineKv3.3     MLSSVCVWSFRGRQGTGKQQPQPVPTPQPPESSPPPLPPPQQQQCSQPGTAASPAGAPLSCGPGGRRAEPCPGLPAVAMGRHGGGGGDSGKIVINVGGVR
BE949391        MLSSVCVWSFRGRQGTGKQQPQPVPTPQPPESSPPPLPPPQQQQCSQPGTAASPAGAPLSCGPGGRRAEPCPGLPAVAMGRHGGGGGDSGKIVINVGGVR
NP_446449(rat)  MLSSVCVWSFSGRQGTRKQHSQPAPTPQPPESSPPPLLPPPQQQCAQPGTAASPAGAPLSCGPGGRRAEPCSGLPAVAMGRHGGGGGDSGKIVINVGGVR
Q63959(mouse)   MLSSVCVWSFRGCQGTGKQQPQPVPTPQPPESSPPPLPPPQQQQCSQPGTGPSP-GVPAFLRPGGRRAEPCPGLPAVAMGRHGGGGGDSGKIVINVGGVR
NP_004968(human) MLSSVCVSSFRGRQGASKQ--QPAPPPQPPESPPPPLPPQQQQPAQPGPAASPAGPPAPRGPGDRRAEPCPGLPAAAMGRHGGGGGDSGKIVINVGGVR
Consensus       MLSSVCVwSFrGrQGtgKQqpQPvPtPQPPESsPPPlpPPqQQQcsQPGtaaSPaG.Pa..gPGgRRAEPCpGLPAvAMGRHGGGGGDSGKIVINVGGVR
```

FIGURE 1. **Amino acid sequence alignment of the cloned mouse Kv3. 3 cDNA with the previously reported Kv3.3 sequence (Q63959) and a mouse EST (BE949391) from GenBank™.** The N terminus of the cDNA sequence investigated in this study had differences in 8 amino acids from the previously reported Kv3.3 (Q63959) cDNA sequence but was identical to an EST BE949391 from the mouse dbEST. In the same N-terminal region, the cDNA sequence differed from the rat sequence (NP_446449) by 9 amino acids and 20 amino acids with the human (NP_004968) sequence. Identical amino acids are shown in *red*. Positions where differences occur are shown in *blue* with the amino acids that differ from the consensus sequence in *black*.

where I_{Na} represents Na^+ current, $I_{Kv3.3}$ and I_{KvLT} represent the Kv3.3 and a Kv1.1-like "low threshold" component of voltage-dependent K^+ current, respectively. I_L is the leak current, and stimuli $I_{ext(t)}$ were presented as step currents (1.0 nA, 0.25 ms) at 200–400 Hz. I_{Na}, I_{KvLT}, and I_L were given by the equations $I_{Na} = -g_{Na}m^3h(50 - V)$, $I_{KvLT} = -g_{LT}\,lr(-80 - V)$ and $I_L = -g_L(-63 - V)$, respectively. To simulate the effect of PKC activation on inactivation of Kv3.3 currents, a slightly different equation was used under control and PKC-stimulated conditions. Under basal (non-PKC activated) conditions, the Kv3.3 current was given by $I_{Kv3.3} = g_{Kv3.3}\,n^3\,(0.23 + 0.77p)(-80 - V)$, whereas after PKC activation Kv3.3 current was given by $I_{Kv3.3} = g_{Kv3.3}\,n^3\,(0.9 + 0.1p)(-80 - V)$. Evolution of the variables m, h, l, r, n, and p were determined by Hodgkin-Huxley-like equations as described previously (26). Parameters for the sodium current were as follows: $g_{Na} = 0.5\ \mu S$, $k_{\alpha m} = 76.4\ ms^{-1}$, $\eta_{\alpha m} = 0.037\ mV^{-1}$, $k_{\alpha m} = 6.93\ ms^{-1}$, $\eta_{\alpha m} = -0.043\ mV^{-1}$, and $k_{\alpha h} = .0001354\ ms^{-1}$, $\eta_{\alpha h} = -0.1216\ mV^{-1}$, $k_{\beta h} = 2.0\ ms^{-1}$, and $\eta_{\beta h} = 0.0384\ mV^{-1}$. Parameters for the low threshold potassium current were as follows: $g_{LT} = 0.02\ \mu S$, $k_{\alpha l} = 1.2\ ms^{-1}$, $\eta_{\alpha l} = 0.03512\ mV^{-1}$, $k_{\beta l} = 0.2248\ ms^{-1}$, $\eta_{\beta l} = -0.0319\ mV^{-1}$, $k_{\alpha r} = 0.0438\ ms^{-1}$, $\eta_{\alpha r} = -0.0053\ mV^{-1}$, $k_{\beta r} = 0.0562\ ms^{-1}$, and $\eta_{\beta r} = -0.0047\ mV^{-1}$. Parameters for the Kv3.3 channel were as follows: $g_{Kv3.3} = 0.15\ \mu S$ (control) or $0.3\ \mu S$ (PKC-activated), $k_{\alpha n} = 0.039\ ms^{-1}$, $\eta_{\alpha n} = 0.0467\ mV^{-1}$, $k_{\beta n} = 0.0868\ ms^{-1}$ $\eta_{\beta n} = 0.0067\ mV^{-1}$, $k_{\alpha p} = 0.000045\ ms^{-1}$, $\eta_{\alpha p} = -0.18925\ mV^{-1}$, $k_{\beta p} = 0.00246\ ms^{-1}$, and $\eta_{\beta p} = 0.01075\ mV^{-1}$. The leakage conductance g_L was 0.002 μS, and C, the cell capacitance, was 0.01 nanofarads.

RESULTS

Cloning of the Kv3.3 Channel from Mouse Brain—Using a RACE-PCR cloning strategy, we have cloned a poly(A)-tailed 2789-bp cDNA corresponding to the full-length mouse Kv3.3 channel cDNA from whole brain of a postnatal 16-day-old mouse. This cDNA was almost identical to the first 2559 bp of the previously reported mouse Kv3.3b nucleotide sequence (GenBank™ accession numbers S69381 and Q63959). When a blast search of the GenBank™ data base at the National Center for Biotechnology Information was performed with the extreme N-terminal sequence, a mouse expressed sequence tag (EST BE949391) was found that matched the new clone and that further extended the 5′-untranslated region sequence by 230 bp. The co-linearity of this cDNA was confirmed by PCR using primers spanning 6–24 bp of inverted BE949391 and 314–332 bp of S69381. This full-length cDNA encodes a 770-amino acid protein that differed from the previously reported

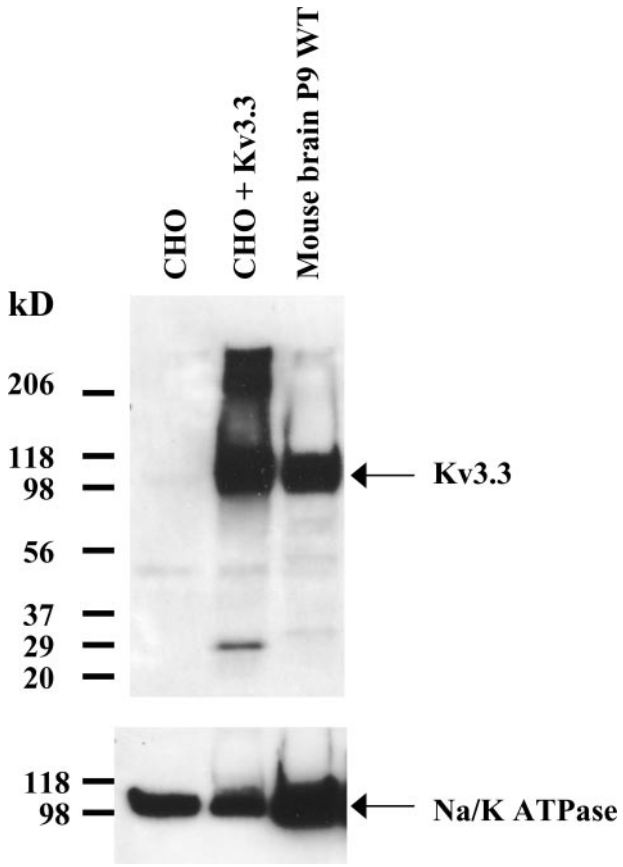

FIGURE 2. **Expression of Kv3. 3 in mouse brainstem.** Anti-Kv3.3 immunoreactive protein from CHO cells transfected with Kv3.3 cDNA has a molecular mass of ~100 kDa, similar to the native anti-Kv3.3 immunoreactive protein from mouse brainstem. No signal was observed in nontransfected CHO cells. Western blot was stripped and re-probed with anti-Na/K-ATPase. Presence of anti-Na/K-ATPase immunoreactive protein in both the CHO cell lanes show approximately equal amounts of protein were loaded. The protein band at ~28 kDa is probably a proteolytic fragment of Kv3.3 channel protein, and the bands at the top of the gel are because of membrane aggregates.

mouse Kv3.3 protein by 8 amino acids in the extreme N terminus as shown in Fig. 1. All other amino acids in the protein were identical to the previously reported mouse Kv3.3b gene (21). We used this new cDNA to characterize the properties of recombinant Kv3.3 channels and to investigate its potential modulation by protein kinase C.

Recombinant and Native Mouse Brain Kv3.3 Proteins Are of Similar Size—In Western blot analysis, an anti-Kv3.3 antibody failed to recognize any specific bands in nontransfected CHO cells, but recognized an ~100-kDa protein in CHO cells over-expressing the cloned Kv3.3 cDNA (Fig. 2). The cloned Kv3.3 protein expressed in CHO cells was also identical in size to the

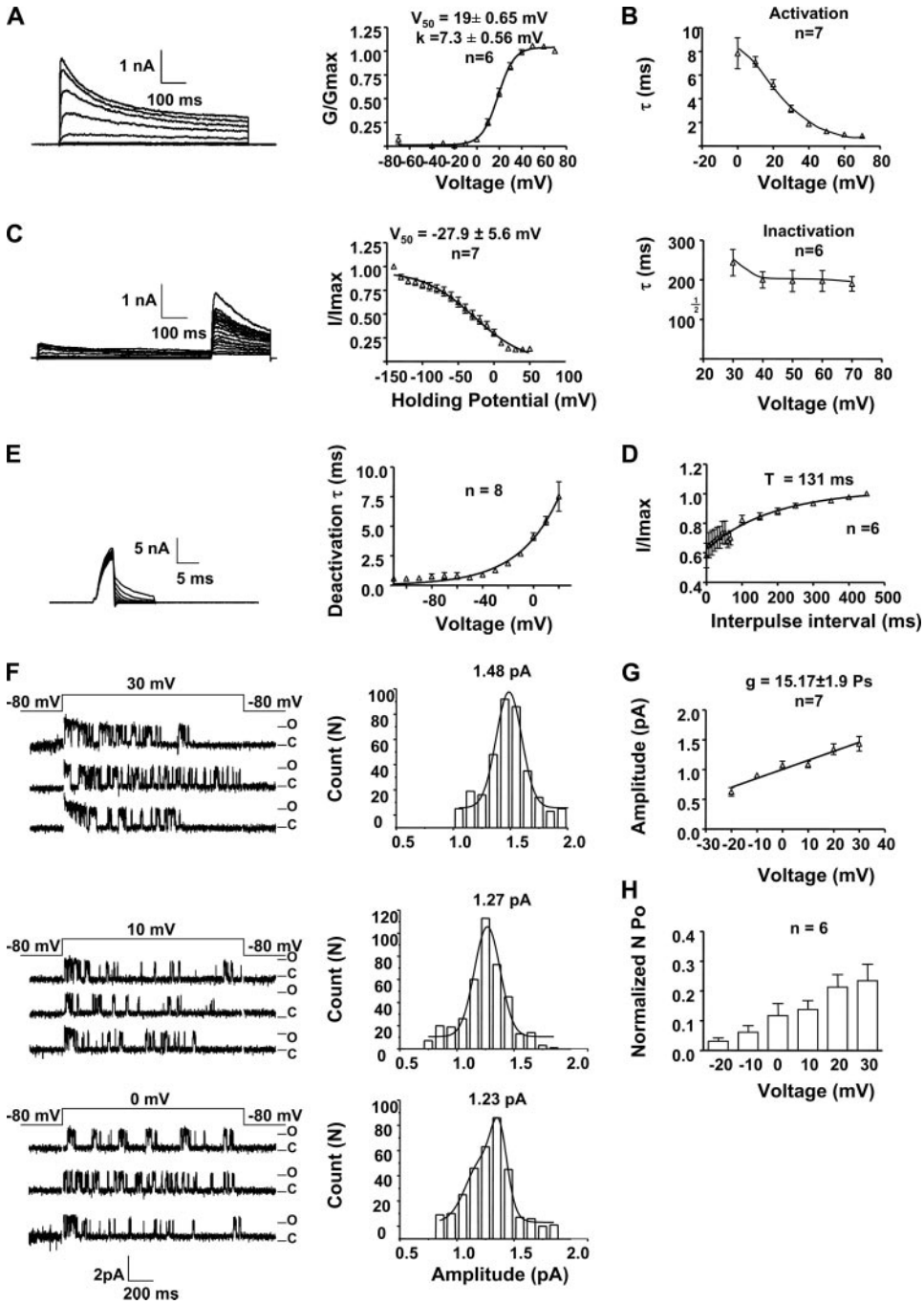

FIGURE 3. **Biophysical properties of Kv3. 3 channels.** *A,* representative current traces and current-voltage relationship for Kv3.3 currents recorded from CHO cells in the whole-cell configuration. Currents were evoked by applying 800-ms voltage steps from a holding potential of −70 to + 70 mV in 10-mV increments. Conductance values were obtained by dividing current with electrochemical driving force ($I_K/(V_m - E_K)$). Normalized conductance-voltage plots were obtained by dividing conductance (*G*) with maximal conductance (G_{max}) and fitting with Boltzmann equation. The plots of τ of activation (*B*, *upper panel*) and τ of inactivation (*B*, *lower panel*) were determined, respectively, by fitting the rising and inactivating phases of currents obtained in *A* with a single term exponential equation. *C,* steady-state inactivation ($h_{730\ ms}$) of Kv3.3 was determined by holding the membrane potential from a pre-pulse potential ranging from −100 to +50 mV in 10-mV increments for 730 ms to a test voltage step of +20 mV for 250 ms. Current amplitude was normalized to the maximum current, and the resulting plot was fit with the Boltzmann equation. *D,* τ of recovery from inactivation was determined by stepping the cells from −100 mV to 20 mV for 2000 ms to a −100-mV step of variable durations in 100- or 7.5-ms increments immediately followed by a test step to 40 mV for 350 ms. Normalized amplitudes (*I*) to maximum (I_{max}) values at 40-mV steps were plotted against the inter-pulse interval and fitted with a single exponential decay equation. *E,* for determining the τ of deactivation, the cells were held at −70 mV, stepped to +50 mV for 5 ms, and then stepped from −110 to 40 mV in 10-mV increments for 10 ms. The deactivating phase of the currents was fit with a single function exponential equation. *F* and *G* show single channel properties of Kv3.3 in CHO cells. *F,* representative cell-attached single channel current traces and their corresponding amplitude histograms at different voltages. Only three of the 10 traces obtained for each voltage are shown; however, all 10 were used for analysis. The patch was held at −80 mV and stepped to different voltages for 1500 ms. *G,* mean current-voltage (*I-V*) relationships of channels obtained by determining current amplitude at first level at different voltages ($n = 7$). The slope of the line fitted on this *I-V* plot is 15.17 ± 1.9 pS. *H,* normalized $N(P_o)$ values determined for different voltages ($n = 6$).

native Kv3.3 protein from mouse brain. In the Kv3.3-transfected CHO cells, we also detected a band at ~28 kDa, which may represent a proteolytic fragment of Kv3.3, and two bands at >200 kDa, which may represent membrane aggregates. As a positive control, we tested for the presence of Na/K-ATPase in all three lanes. The blot was stripped and reprobed with anti-Na/K-ATPase antibodies (Fig. 2, *lower panel*). Both the transfected and nontransfected CHO cell lanes contain equal amounts of Na/K-ATPase protein (~100 kDa).

Biophysical Properties of Recombinant Kv3.3 Channels in CHO Cells—We first used CHO cells overexpressing the Kv3.3 cDNA to characterize its biophysical properties, including its voltage dependence and kinetics of activation, steady-state inactivation, and recovery from inactivation. In Kv3.3-expressing cells, 800-ms voltage steps from a holding potential of −70 to + 70 mV in 10-mV increments evoked outward currents that were rapidly activating (τ less than 2 ms at 40 mV and above; Fig. 3*B, upper panel*) and with a $V_{½}$ of activation of 19 ± 0.65 mV and a slope factor of 7.3 ± 0.56 mV, $n = 6$ (Fig. 3*A*). These currents also inactivated with a τ of ~200 ms at voltages above 40 mV ($n = 6$) (Fig. 3*B, lower panel*). Inactivation was also incomplete, with ~32% residual current after long depolarizing pulses to +50 mV (Fig. 3*A*).

Half-maximal inactivation ($h_{730\ ms}$) for Kv3.3 was determined to be −27.9 ± 5.6 mV ($n = 7$) by measuring currents evoked by stepping from potentials between −100 and +50 mV to a test voltage of +20 mV (Fig. 3*C*). The time constant for recovery from inactivation at −100 mV was determined using a two-pulse protocol. Kv3.3 currents were first inactivated by stepping the cells from −100 to 20 mV for 2000 ms. This was followed by a step to −100 mV for variable durations up to 500 ms (in 7.5 or 100 ms increments) followed by a test pulse to 40 mV for 350 ms. Normalized amplitudes (I) to maximum (I_{max}) values at 40 mV were plotted against the inter-pulse interval and fitted with a single exponential decay equation. The half-life of recovery from inactivation of Kv3.3 channels is 131 ms ($n = 6$) (Fig. 3*D*).

To determine the time constant of deactivation, cells were held at −70 mV, stepped to +50 mV for 5 ms, and then stepped from −110 to 40 mV in 10-mV increments for 10 ms. The τ of deactivation ranged from 2 to 8 ms for voltages between −20 to +20 mV (Fig. 3*E*).

Further characterization of Kv3.3 channels in CHO cells was carried out using single channel recordings in the cell-attached configuration. Representative single channel current traces with their respective amplitude histograms for different voltages are shown in Fig. 3*F*. The single channel conductance of Kv3.3 channels in cell-attached configuration is 15.2 ± 1.9 pS (Fig. 3*G*). The opening of Kv3.3 channel is voltage-dependent as determined by the increase in NP_o (number of channels × probability of opening) at more depolarized potentials (Fig. 3*H*). Kv3.3 channels begin to activate at approximately −20 mV as is the case for other members of the Kv3 family. Some patches (such as that in Fig. 3*F*) contained only a single channel, as determined by openings to only a single current level at positive potentials (+30 mV). This enabled us to perform open and close-dwell time analysis. At more negative potentials, Kv3.3 channel openings could fit with a single open state (with a dwell time of ~5.6 ms at 0 mV). At more depolarized potentials, two open states could be resolved (mean open times 1.8 and 12.3 ms at +30 mV). Kv3.3 channel closings could only be fit with two or three closed states at all voltages tested (data not shown).

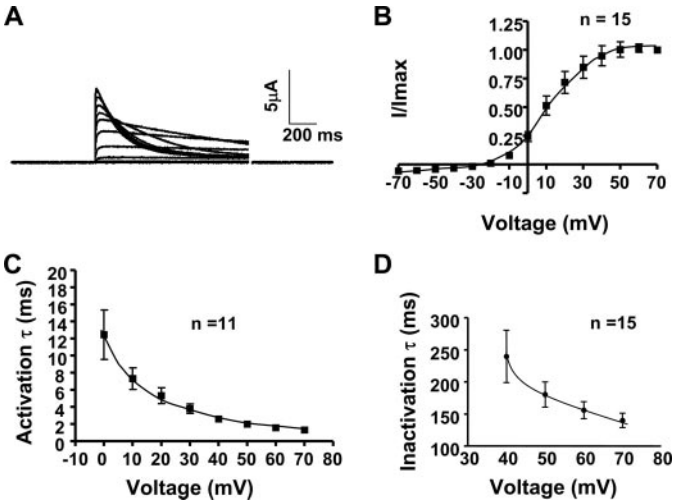

FIGURE 4. **Current-voltage relationship of Kv3. 3 currents in *Xenopus* oocytes.** *A,* representative current traces for Kv3.3 currents expressed in *Xenopus* oocytes. Currents were obtained by applying 1000-ms voltage steps from a holding potential of −80 to +70 mV in 10-mV increments. *B,* current-voltage relationship. Peak current amplitude at each voltage step was divided by maximum current amplitude obtained at +70 mV and was plotted against the applied voltage. Kv3.3 currents start to activate at voltages more positive of −20 mV. The plots of τ of activation (*C*) and inactivation (*D*) were obtained, respectively, by fitting the rising and inactivating phases of the currents in *A* with a single term exponential equation. At 40 mV, the Kv3.3 currents activate within 2.6 ± 0.26 ms and inactivate within 359.5 ± 83.8 ms.

PKC Activators Increase Current Amplitudes and Slow Inactivation of Kv3.3—The dialysis of intracellular components during whole-cell patch clamp recordings is known to adversely compromise modulation of channels by PKC (2, 14, 27). To investigate the modulation of Kv3.3 channels by this enzyme, we therefore expressed Kv3.3 in *Xenopus* oocytes and assayed currents using the less invasive dual-microelectrode voltage clamp technique. Currents in Kv3.3 cRNA-injected oocytes were detected at potentials more positive than approximately −20 mV and had activation kinetics similar to those recorded in transfected CHO cells (Fig. 4, *A–C*). As in the CHO cells, Kv3.3 currents in oocytes inactivated during 1-s depolarizing commands to positive potentials, although their rate of inactivation was slightly greater than in the mammalian cells (with a time constant of 155.8 ± 14.1 ms at 70 mV (Fig. 4*D*)). The rate of inactivation of Kv3.3 currents in *Xenopus* oocytes was also voltage-dependent, with the value of time constant decreasing with increasing voltages.

To investigate the modulation of Kv3.3 channels by PKC, we tested several structurally distinct activators of this enzyme, including Bryostatin1 (28) and pseudoRack1 (29). Application of 10 nM Bryostatin1 for 20 min to oocytes expressing Kv3.3 currents resulted in a loss of the inactivation normally observed at voltages between 40 and 70 mV and increased peak amplitudes (Fig. 5, *A* and *B*). Because in many cases, little or no inactivation could be measured after Bryostatin1 treatment, it was not possible to quantify time constants for inactivation. To provide a measure of the loss of inactivation, we therefore scaled

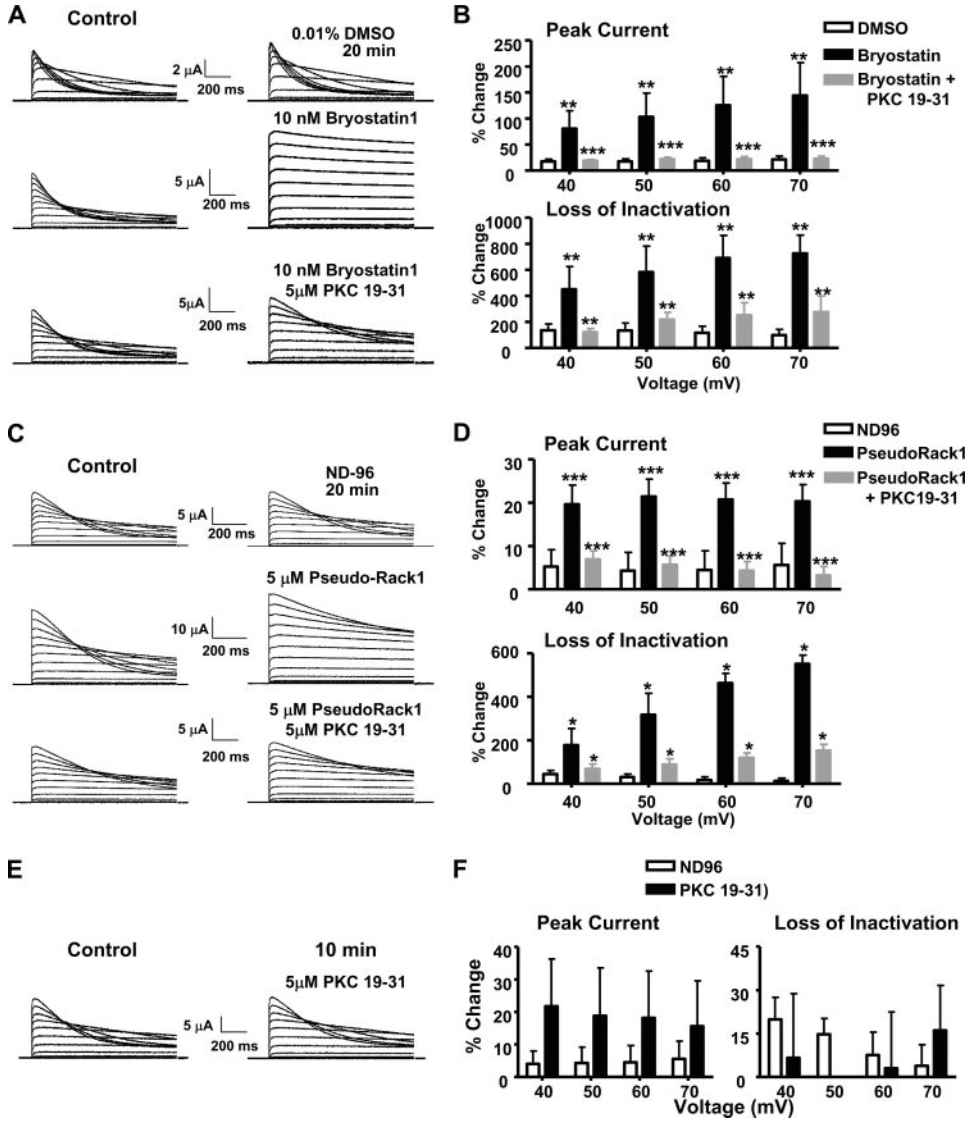

FIGURE 5. **Bryostatin-1 and PseudoRack1 increase peak current amplitudes and remove inactivation of Kv3. 3 currents, and pretreatment with PKC-(19–31) peptide reduces their effect.** *A,* representative traces of Kv3.3 currents in *Xenopus* oocytes before and 20 min after exposure to the solvent DMSO (0.01%) (*upper trace*), to 10 nM Bryostatin-1 (*middle trace*), or pretreatment with PKC-(19–31) for 10 min before application of Bryostatin1 for 20 min (*lower trace*). *C,* representative traces of Kv3.3 currents in *Xenopus* oocytes before and 20 min after exposure to PseudoRack1 (5 μM) (*middle traces*) or after addition of the buffer ND-96 alone or after exposure to PKC-(19–31) for 10 min prior to the application of PseudoRack1 for 20 min (*lower trace*). *E,* representative traces of Kv3.3 currents before and after the application of PKC-(19–31) for 10 min. *B, D,* and *F,* quantification of the responses of Kv3.3 currents to 10 nM Bryostatin-1 (*B*, $n = 7$) or 5 μM PseudoRack1 (*D*, $n = 4$) or 5 μM PKC-(19–31) (*F*, $n = 9$) and the response of Kv3.3 currents to these PKC activators in the presence of PKC pseudosubstrate PKC-(19–31) ($n = 4$ and 6 for Bryostatin-1 and PseudoRack1, respectively). For application of ND-96 alone (*F*), $n = 4$. Kv3.3 currents were measured by applying voltage commands from a holding potential of −80 mV to +40, +50, +60, and +70 mV for a duration of 1000 ms. Peaks currents were measured at the start (10–60 ms) of the commands, and loss of inactivation was calculated as described in the text. For statistical analysis of the effect of activators alone, the changes in current amplitudes and inactivation of oocytes treated with the activators were compared with the drug vehicle. For statistical analysis of the effect of activators in the presence of inhibitory peptide PKC-(19–31), comparisons are between the effect of the activators alone and those of the same activators in the presence of PKC-(19–31). *, $p < 0.05$; **, $p < 0.01$; ***, $p < 0.001$.

the peak currents before and after Bryostatin1 treatment and then calculated the percentage increase in current near the end of a 1-s depolarizing command (Fig. 5*B*). With this protocol, an increase in current with no change in kinetic behavior provides an increase in peak current but no loss of inactivation. The increase in peak currents and loss of inactivation 20 min after Bryostatin1 treatment were highly significant ($p < 0.006$, $n = 7$), whereas no significant effect was found when 0.01% DMSO, the solvent for Bryostatin1, was applied to the cells (Fig. 5, *A* and *B*).

We next tested the effect of pseudoRack1, a peptide activator of PKC attached to a cell permeabilization vector peptide (Fig. 5, *C* and *D*). As with Bryostatin1, 20 min after application of pseudoRack1, Kv3.3 peak current was increased ($p < 0.0002$, $n = 4$), and the rate of inactivation of the currents was also significantly reduced ($p < 0.03$) (Fig. 5, *C* and *D*). No change in current was observed over time when cells were maintained in ND-96, the solvent medium for pseudoRack1 (Fig. 5, *C* and *D*).

The Pseudosubstrate Peptide PKC-(19–31) Inhibits the Action of PKC Activators—To determine whether the effects of PKC activators on Kv3.3 currents are mediated through phosphorylation by PKC, we tested the actions of the PKC inhibitory peptide PKC-(19–31), a specific pseudosubstrate inhibitory peptide inhibitor (30). We applied PKC-(19–31) for 10 min prior to the application of PKC activators. As was the case for PseudoRack1, the PKC inhibitory peptide was linked to a cell permeabilization vector for uptake by the oocytes. Application of 5 μM PKC-(19–31) alone for 10 min had little effect on Kv3.3 currents (Fig. 5, *E* and *F*). The presence of the inhibitor, however, significantly blocked the effects of subsequent application of either Bryostatin1 or PseudoRack1 on both peak amplitudes ($p < 0.0009$ and $p < 0.0005$, respectively) and inactivation ($p < 0.006$ and $p < 0.025$, respectively) of Kv3.3 currents (Fig. 5, *A–D*).

Serines at Positions 3 and 9 on the Kv3.3 Channel Protein Are Potential PKC Phosphorylation Sites—To determine whether the inactivation of Kv3.3 that is sensitive to PKC activation represents N-type inactivation, we constructed a Kv3.3 mutant in which the first 78 amino acids were deleted (Δ78). Consistent with classical N-type inactivation, this N-terminal truncation produced noninactivating currents that did not respond to Bryostatin1 (Fig. 6). Because most of the known PKC phosphorylation sites on potassium channels are on serine residues, we focused on the nine serine residues on the N-terminal domain of Kv3.3. To identify specific putative regulatory

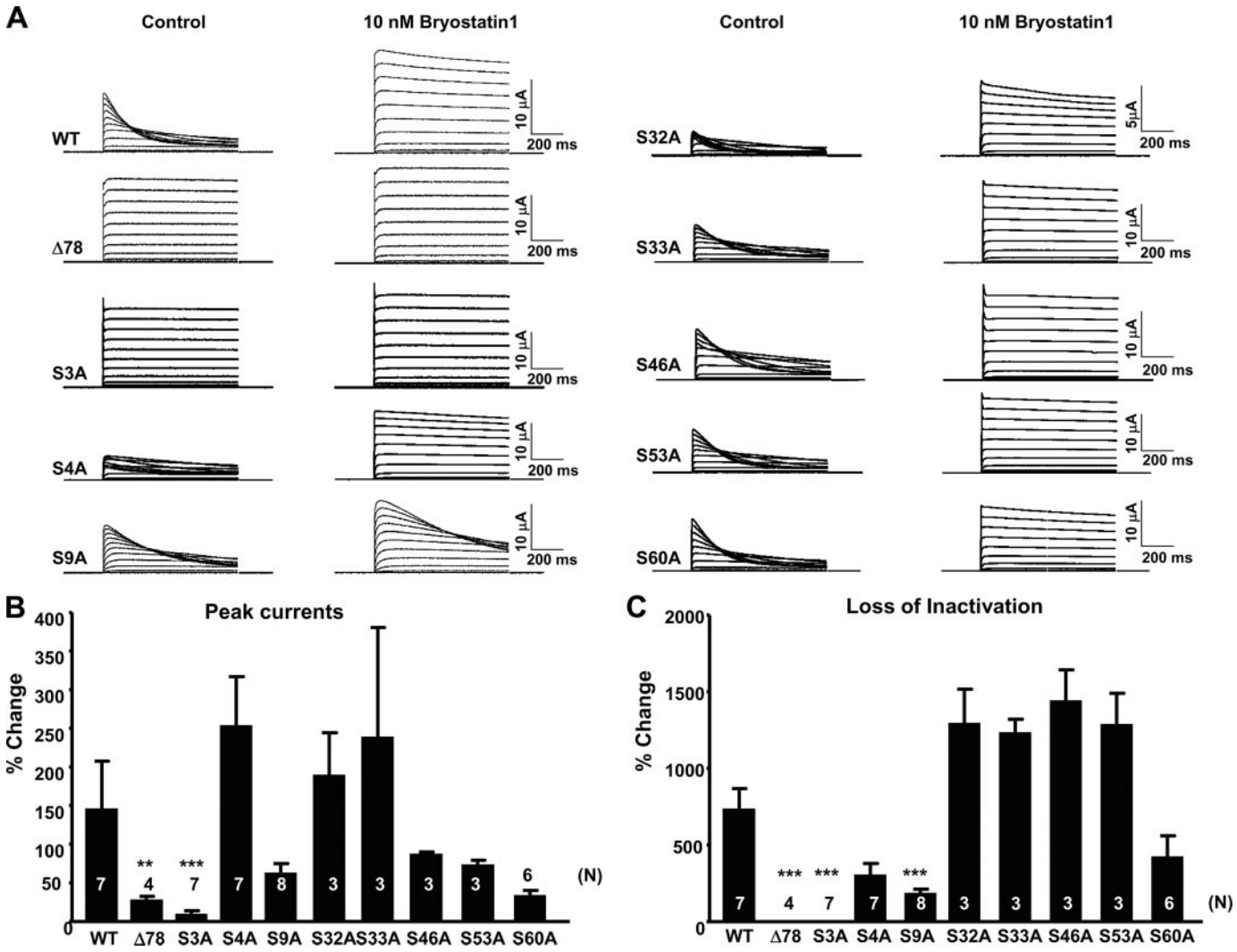

FIGURE 6. **Effect of PKC activator Bryostatin1 on Kv3. 3 mutants.** *A,* representative current traces of Kv3.3 mutants, Δ78, S3A, S4A, S9A, S32A, S33A, S46A, S53A, and S60A, and the effect of Bryostatin1 on peak currents and on inactivation of current after 20 min of drug application. Δ78 and S3A produce noninactivating currents. Some mutations (*e.g.* S3A) produced currents in which rapid activation was followed by a very rapid (~20 ms) but only partial decline to a steady state, as has also been described for wild type Kv3.1 currents (31). *B,* group data for the effects of Bryostatin1 on peak currents of wild type Kv3.3 channels and on Kv3.3 mutants Δ78, S3A, S4A, S9A, S32A, S33A, S46A, S53A, and S60A. For simplicity only currents evoked in response to voltage commands to +70 mV are quantified. *C,* group data for the effects of Bryostatin1 on the inactivated component of currents at +70 mV for the same mutants as in *B*. Data were analyzed as described in Fig. 5. For statistical analyzes, the change in peak currents and loss of inactivation of currents for the different mutant Kv3.3 channels were compared with those for the wild type Kv3.3 channels. **, $p < 0.01$; ***, $p < 0.005$. Numbers of observations (*N*) are indicated on the *bar graphs*.

phosphorylation sites, we mutated each of these serine residues individually to alanines and tested their response to Bryostatin1. Although there was some variability in the degree to which different mutants responded to the PKC activator, only two of these mutations had responses that were statistically significantly different from those of wild type channels, and both mutations were at the very N terminus of the protein. Mutation of serine 3 had an effect that was identical to that of the full N-terminal truncation. S3A currents did not inactivate during the depolarizing command and were completely unresponsive to Bryostatin1 (Fig. 6). In contrast, mutation of serine 9 to an alanine produced currents that did inactivate during depolarization, but the effect of Bryostatin1 on the rate of inactivation was very significantly attenuated compared with wild type channels, as indicated by the reduced effect of Bryostatin1 on the degree of loss of inactivation (Fig. 6). Fig. 6*A* shows examples of individual current responses of the mutant to the PKC activator and Fig. 6, *B* and *C*, shows group data for the increases in peak and sustained components of current measured at a test potential of +70 mV.

To further characterize the role of serine 3 in the control of inactivation, we constructed three additional mutations at this site, replacing the serine with threonine (S3T), cysteine (S3C), or aspartate (S3D). Threonine and cysteine are close in structure to serine and are also both polar and neutral. They differ, however, in that the threonine is a good substrate for phosphorylation by PKC, whereas mutation to cysteine prevents phosphorylation. Like wild type currents, currents of the S3T mutant inactivated during depolarization. Moreover, treatment with Bryostatin1 strongly reduced inactivation, increasing both peak current and the loss of inactivation parameter for the S3T current (Fig. 7, *A* and *B*). In contrast, S3C currents were noninactivating and showed no significant response to Bryostatin1 (Fig. 7, *A* and *B*). Substitution of serine with a negatively

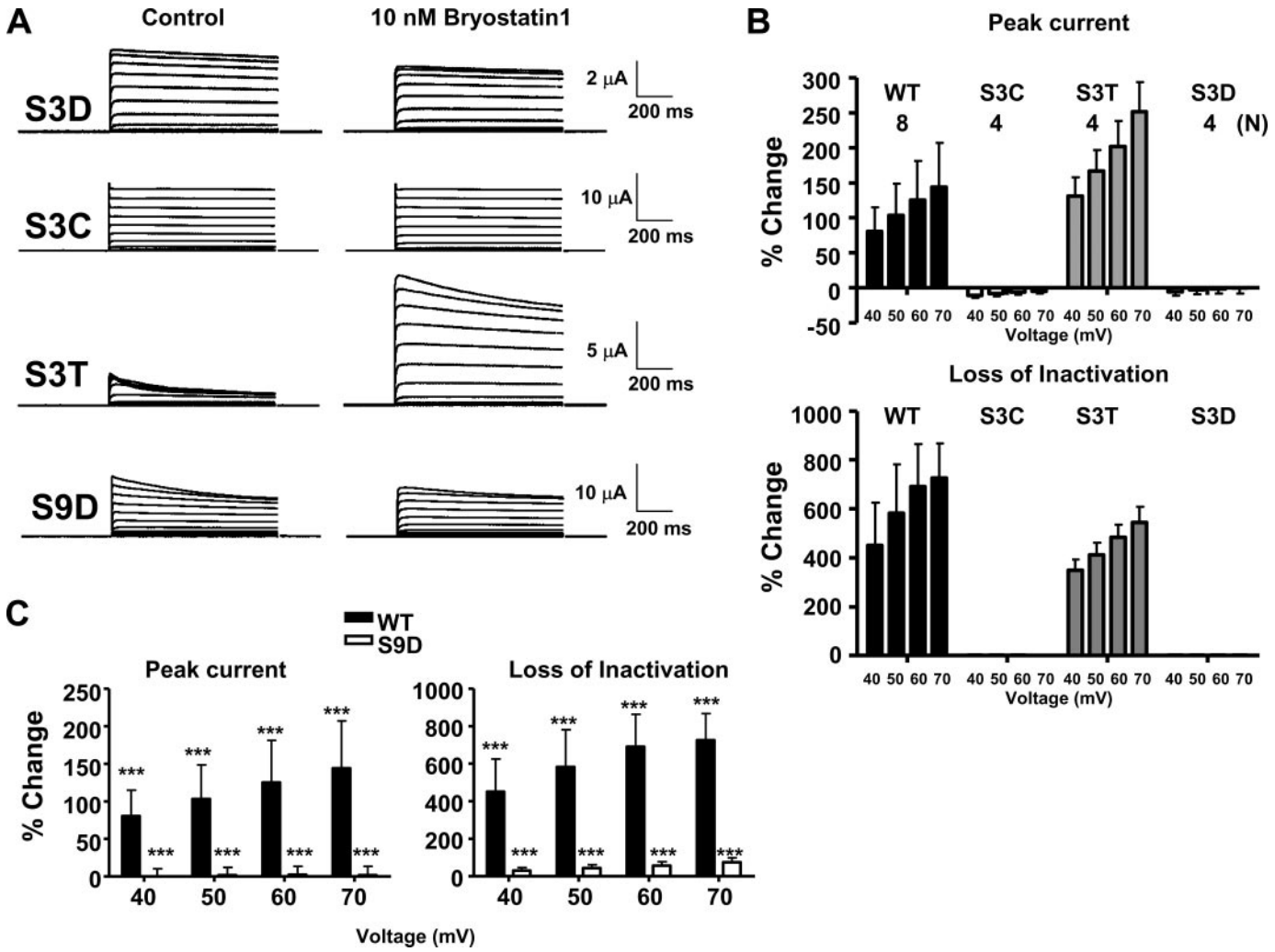

FIGURE 7. **Effect of PKC activator Bryostatin1 on Kv3. 3 mutants S3D, S3C, S3T, and S9D.** *A,* representative current traces of Kv3.3 mutants S3D, S3C, S3T, and S9D before and 20 min after exposure to Bryostatin1. Like S3A, S3D and S3C also produced noninactivating currents, and application of Bryostatin1 caused a small decrease in the peak current amplitudes at the different voltages tested. The response of mutant S3T Kv3.3 channels was similar to that of wild type Kv3.3 channels. *B,* group data for the effects of Bryostatin1 on peak and inactivated components of current at +40, +50, +60, and +70 mV for mutations at serine 3 (S3D, S3C, and S3T). *C,* group data for the effects of Bryostatin1 on peak and loss of inactivation of current for the S9D mutation ($n = 8$ and 5 for wild type and S9D, respectively). ***, $p < 0.0005$. Protocols for measurements of peak and loss of inactivation of current are as described in the text.

charged aspartate residue would be expected to mimic the electrostatic effects of phosphorylation. The mutant S3D also produced noninactivating currents that were completely unresponsive to Bryostatin1 (Fig. 7, *A* and *B*). These findings are consistent with the hypothesis that a hydroxyl group on residue 3 is required for inactivation and that elimination of this group either by phosphorylation or by mutation suppresses inactivation of Kv3.3 channels.

As described above, the mutant S9A had a statistically significantly reduced response to Bryostatin1. In contrast to S3A, however, S9A inactivated during depolarization, although the time constant was longer than that of wild type channels (514 ± 85 ms at 70 mV for S9A, $n = 5$, *versus* 156 ± 14 ms for wild type, $n = 15$). To characterize this site further, we substituted this serine with aspartic acid to mimic the negative charge of phosphorylation (Fig. 7). The inactivation kinetics of this mutant S9D (561 ± 131 ms at 70 mV, $n = 5$) were similar to those of S9A. Moreover, this S9D mutation resulted in a very severe attenuation of the response to Bryostatin1 (Fig. 7, *A* and *C*). These findings are consistent with the hypothesis that, in addition to serine 3, phosphorylation of serine 9 plays a role in regulating the rate of inactivation of Kv3.3 channels.

Computer Simulations of Kv3.3 Modulation in Rapidly Firing Neurons—To investigate the potential effects of modulation of Kv3.3 amplitude and kinetics in rapidly firing neurons, we carried out numerical simulations. We used a previously described model of neurons of the MNTB (3, 26) to simulate the effects of PKC-dependent modulation of Kv3.1 channels, the dominant high threshold potassium current in the somata of these cells (2, 3, 14, 31). The Kv3.1-like current in this model was replaced by a current that matched Kv3.3 in its voltage dependence and kinetics of activation and inactivation, and simulations were carried out using Kv3.3-like currents that either matched those in control cells or those exposed to activators of PKC (Fig. 8*A*). The model neurons were stimulated with repeated intracellular current pulses applied at frequencies up to 400 Hz. At lower stimulus frequencies, at which each stimulus evoked an action potential (*200 Hz* in Fig. 8*B*), there was little difference between

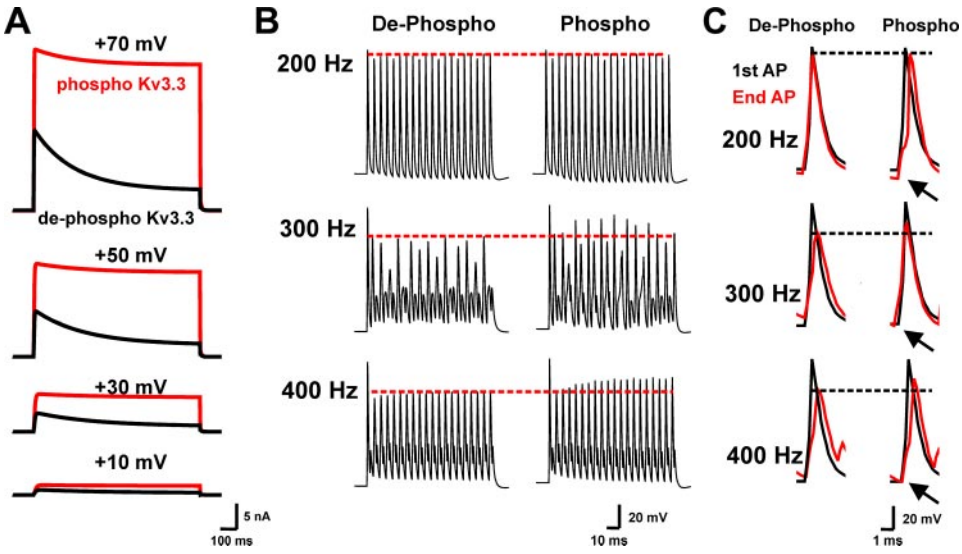

FIGURE 8. **Numerical simulations of the effects of control and PKC-activated Kv3. 3 currents on firing of a model fast-firing neuron.** *A,* simulated control (de-phospho) and PKC-activated (phospho) Kv3.3 currents evoked by test depolarizations to +10, +30, +50, and +70 mV. *B,* response of the model neuron to trains of depolarizing current pulses (1.0 nA, 0.25 ms) applied at frequencies of 200, 300, and 400 Hz. *Horizontal dashed red line* is aligned at the height of the last action potential evoked in a cell with control (de-phospho) Kv3.3 current (*left traces*), and demonstrates that action potential height at 300 and 400 Hz is higher with simulated PKC-activated (phospho) Kv3.3 currents (*right traces*). *C,* superimposition of the first (*black*) and last (*red*) evoked action potentials in response to the same trains as in *B*. Under PKC-activated (phospho) conditions, the later action potentials are systematically higher than in de-phospho conditions, and repolarization between action potentials (indicated by *arrows*) is enhanced under conditions of PKC activation.

the firing patterns observed with the "de-phosphorylated" and "phosphorylated" Kv3.3 currents, except that hyperpolarizations that follow each action potential were larger with the phosphorylated channel (Fig. 8*C*, *200 Hz*). As the stimulus frequency was increased, however, not all stimulus pulses evoked an action potential (Fig. 8*B*). At these higher stimulus frequencies, the height of action potentials during the trains was always higher in simulations with the larger Kv3.3 "PKC-phosphorylated" currents (Fig. 8, *B* and *C*, *300* and *400 Hz*). These simulations suggest that, by increasing the rate of repolarization of action potentials, increases in Kv3.3 currents such as those produced by PKC activation may help to maintain action potential height during high frequency stimulation.

DISCUSSION

In this study we have characterized the biophysical characteristics and modulation of Kv3.3 channels heterologously expressed from a mouse brainstem DNA clone. We have found that N-type inactivation of these channels is abolished by activators of PKC and that this effect can be prevented by a specific pseudosubstrate peptide inhibitor of PKC. Furthermore, we identified two serine residues, Ser-3 and Ser-9, located in consensus PKC phosphorylation sites at the N terminus of the Kv3.3 protein that are required for the regulation of the channel by PKC.

An early review article (12) reported that when recombinant Kv3.3 channels are expressed in mammalian cells such as human embryonic kidney cells, they produce noninactivating currents, but that expression of the same channels in *Xenopus* oocytes gives rise to A-type inactivating currents similar to those that were found in this study using either CHO cells or oocytes. Human Kv3.3 channels expressed in CHO cells also give rise to inactivating currents (32). A previous study investigating differences in the inactivation rates of Kv3.3 currents when expressed heterologously in different mammalian cells suggested that differences in inactivation can result from differences in the choice of the N-terminal methionine residue at which translation begins (33). Lack of inactivation was attributed to the use of a second start methionine in the N-terminal domain, producing truncated Kv3.3 channels that did not have N-type inactivation. These investigators also found that when the nucleotide sequence surrounding the first methionine start site was mutated to one more closely resembling a strong consensus Kozak sequence, Kv3.3 currents had rapid voltage-dependent inactivation in all expression systems assayed. Our present results suggest an additional possibility for the differences observed in the rates of current inactivation in different expression system. Such observed disparity may also be due to the presence of varying levels of basal PKC activity, leading to differential phosphorylation of Kv3.3 channels in distinct cells. It is possible that both of these mechanisms, translation from a different methionine start site and phosphorylation of N terminus by PKC, may be used by cells expressing native Kv3.3 channels for fine control of Kv3.3 current inactivation in a tissue-specific or activity-dependent manner.

This study has also established some of the biophysical properties of murine Kv3.3 channels. Like other members of the Kv3 family, murine Kv3.3 channels display rapid activation and deactivation kinetics and a high threshold of voltage activation. Rates of activation and inactivation of mouse Kv3.3 channels are quantitatively similar to those of the full-length human Kv3.3 channel, although their rate of deactivation is approximately twice as fast as that reported for the human channels (32). Somewhat greater differences are seen when comparing the properties of murine Kv3.3 channels with those of previously described *Apteronotus* Kv3.3 channels quantified in CHO cells (33). For example, murine Kv3.3 channels have a much slower τ of inactivation at 30 mV (~240 ms) as compared with ~90 ms for the *Apteronotus* Kv3.3 channels, and the $V_{½}$ of activation of murine Kv3.3 channels is 19 mV, whereas that for the *Apteronotus* channels is 7.6 mV. These differences likely reflect species differences in amino acid sequence. We have also characterized the single channel properties of the murine Kv3.3 channels. The single channel conductance in our experimental conditions using physiological solutions was about 15 pS, which is again different from the previously reported *Apteronatus* Kv3.3 (33) and human Kv3.3 single channel conductance values

of ~38 pS (32). However, the single channel conductance measured in our experiments is similar to that previously reported for mammalian Kv3.3 channels in physiological solutions (12). The detailed characterization of the electrophysiological properties of murine Kv3.3 channels will be helpful in isolating the Kv3.3 current in neurons and understanding their unique contribution to the physiology of these cells.

Our present experiments suggest that phosphorylation of N-terminal serine residues of the Kv3.3 channel protein by PKC removes the N-type inactivation of Kv3.3 currents, a finding that resembles the actions of PKC modulation on Kv3.4 channels (15). Previous studies have indicated that N-type "ball and chain" inactivation in *Shaker*-type K^+ channels requires the first ~10 amino acids at the N terminus to be hydrophobic and for the next 10 to be hydrophilic with excess positive charge (34–36). Based on the crystal structure of KcsA K^+ channel, the sixth membrane-spanning segment of voltage-dependent K^+ channels is thought to line the pore on the intracellular side of the selectivity filter. This region of the pore forms a 10-Å-wide central cavity that gradually tapers to about 4 Å near the cytoplasmic opening (37). Structural studies combined with mutagenesis have suggested that the N-terminal inactivation ball enters the inner pore and lodges in the central cavity such that the first three amino acids of the N terminus bind in the cavity (34). The sequence of the N terminus of murine Kv3.3 channels is fully consistent with this model of inactivation. Moreover, phosphorylation of one or two serine residues in the first 10 amino acids would confer an excess of negative charge and therefore would prevent the N terminus from entering the pore, resulting in a loss of inactivation. Removal of inactivation by phosphorylation at position Ser-3 and Ser-9 on Kv3.3 channels is therefore consistent with this hypothesis.

Simple computer modeling of a fast firing neuron with Kv3.3 currents suggested that changes in the amplitude or kinetics of Kv3.3 channels are likely to have a selective effect on the firing properties of neurons when they are firing action potentials at high rates. A higher level of Kv3.3 current, such as occurs upon PKC activation, allowed the model neurons to maintain action potential height during stimulation at high frequencies. The specific rate at which the currents inactivate during maintained depolarization is, however, unlikely to influence the response of the neurons to short stimulus trains (<1 s). In particular, because significant inactivation occurs only at positive potentials (>+30 mV), the degree of inactivation expected during short bursts of action potentials is minimal. Thus, although we found differences in inactivation between Kv3.3 currents in CHO cells and oocytes, the specific rate of inactivation does not significantly impact the conclusions of our computer modeling data for auditory neurons. Our results are generally consistent with recordings from Kv3.3 knock-out mice, which reveal that cerebellar Purkinje neurons fire at low rates in the absence of Kv3.3 channels (38). If Kv3.3 channels are located at nerve terminals (18, 39), however, modulation of current amplitude might be expected indirectly to alter calcium influx and to have a profound effect on neurotransmitter release in the absence of overt changes in firing patterns.

Acknowledgment—We thank Deirdre Stewart for advice throughout the study, critical comments on the manuscript, and for frog surgery.

REFERENCES

1. Rudy, B., and McBain, C. J. (2001) *Trends Neurosci.* **24,** 517–526
2. Song, P., Yang, Y., Barnes-Davies, M., Bhattacharjee, A., Hamann, M., Forsythe, I. D., Oliver, D. L., and Kaczmarek, L. K. (2005) *Nat. Neurosci.* **8,** 1335–1342
3. Wang, L. Y., Gan, L., Forsythe, I. D., and Kaczmarek, L. K. (1998) *J. Physiol. (Lond.)* **509,** 183–194
4. Kaczmarek, L. K., Bhattacharjee, A., Desai, R., Gan, L., Song, P., von Hehn, C. A., Whim, M. D., and Yang, B. (2005) *Hear. Res.* **206,** 133–145
5. Brownell, W. E. (1975) *Brain Res.* **94,** 413–433
6. Wu, S. H., and Kelly, J. B. (1993) *Hear. Res.* **68,** 189–201
7. Smith, P. H., Joris, P. X., and Yin, T. C. (1998) *J. Neurophysiol.* **79,** 3127–3142
8. Taschenberger, H., and von Gersdorff, H. (2000) *J. Neurosci.* **20,** 9162–9173
9. Brand, A., Behrend, O., Marquardt, T., McAlpine, D., and Grothe, B. (2002) *Nature* **417,** 543–547
10. Kopp-Scheinpflug, C., Lippe, W. R., Dorrscheidt, G. J., and Rubsamen, R. (2003) *J. Assoc. Res. Otolaryngol.* **4,** 1–23
11. Misonou, H., Mohapatra, D. P., Park, E. W., Leung, V., Zhen, D., Misonou, K., Anderson, A. E., and Trimmer, J. S. (2004) *Nat. Neurosci.* **7,** 711–718
12. Rudy, B., Chow, A., Lau, D., Amarillo, Y., Ozaita, A., Saganich, M., Moreno, H., Nadal, M. S., Hernandez-Pineda, R., Hernandez-Cruz, A., Erisir, A., Leonard, C., and Vega-Saenz de Miera, E. (1999) *Ann. N. Y. Acad. Sci.* **868,** 304–343
13. Macica, C. M., and Kaczmarek, L. K. (2001) *J. Neurosci.* **21,** 1160–1168
14. Macica, C. M., von Hehn, C. A., Wang, L. Y., Ho, C. S., Yokoyama, S., Joho, R. H., and Kaczmarek, L. K. (2003) *J. Neurosci.* **23,** 1133–1141
15. Covarrubias, M., Wei, A., Salkoff, L., and Vyas, T. B. (1994) *Neuron* **13,** 1403–1412
16. Moreno, H., Kentros, C., Bueno, E., Weiser, M., Hernandez, A., Vega-Saenz de Miera, E., Ponce, A., Thornhill, W., and Rudy, B. (1995) *J. Neurosci.* **15,** 5486–5501
17. Li, W., Kaczmarek, L. K., and Perney, T. M. (2001) *J. Comp. Neurol.* **437,** 196–218
18. Chang, S. Y., Zagha, E., Kwon, E. S., Ozaita, A., Bobik, M., Martone, M. E., Ellisman, M. H., Heintz, N., and Rudy, B. (2007) *J. Comp. Neurol.* **502,** 953–972
19. Frohman, M. A. (1995) in *PCR Primer: A Laboratory Manual* (Dieffenbach, C. W., and Dveksler, G. S., eds) pp. 381–409, Cold Spring Harbor Laboratory Press, Cold Spring Harbor, NY
20. Ghanshani, S., Pak, M., McPherson, J. D., Strong, M., Dethlefs, B., Wasmuth, J. J., Salkoff, L., Gutman, G. A., and Chandy, K. G. (1992) *Genomics* **12,** 190–196
21. Goldman-Wohl, D. S., Chan, E., Baird, D., and Heintz, N. (1994) *J. Neurosci.* **14,** 511–522
22. Corpet, F. (1988) *Nucleic Acids Res.* **16,** 10881–10890
23. Forman, S. A. (1997) *Biophys. J.* **72,** 2170–2179
24. Liu, S. Q., and Kaczmarek, L. K. (1998) *J. Neurosci.* **18,** 8758–8769
25. Richardson, F. C., and Kaczmarek, L. K. (2000) *Hear. Res.* **147,** 21–30
26. Perney, T. M., and Kaczmarek, L. K. (1997) *J. Comp. Neurol.* **386,** 178–202
27. Strong, J. A., Fox, A. P., Tsien, R. W., and Kaczmarek, L. K. (1987) *Nature* **325,** 714–717
28. Lorenzo, P. S., Bogi, K., Acs, P., Pettit, G. R., and Blumberg, P. M. (1997) *J. Biol. Chem.* **272,** 33338–33343
29. Ron, D., and Mochly-Rosen, D. (1995) *Proc. Natl. Acad. Sci. U. S. A.* **92,** 492–496
30. House, C., and Kemp, B. E. (1987) *Science* **238,** 1726–1728
31. Kanemasa, T., Gan, L., Perney, T. M., Wang, L. Y., and Kaczmarek, L. K. (1995) *J. Neurophysiol.* **74,** 207–217
32. Rae, J. L., and Shepard, A. R. (2000) *Exp. Eye Res.* **70,** 339–348
33. Fernandez, F. R., Morales, E., Rashid, A. J., Dunn, R. J., and Turner, R. W.

(2003) *J. Biol. Chem.* **278,** 40890–40898
34. Zhou, M., Morais-Cabral, J. H., Mann, S., and MacKinnon, R. (2001) *Nature* **411,** 657–661
35. Hoshi, T., Zagotta, W. N., and Aldrich, R. W. (1990) *Science* **250,** 533–538
36. Zagotta, W. N., Hoshi, T., and Aldrich, R. W. (1990) *Science* **250,** 568–571
37. Doyle, D. A., Morais Cabral, J., Pfuetzner, R. A., Kuo, A., Gulbis, J. M., Cohen, S. L., Chait, B. T., and MacKinnon, R. (1998) *Science* **280,** 69–77
38. Akemann, W., and Knopfel, T. (2006) *J. Neurosci.* **26,** 4602–4612
39. Desai, R., Joho, R. H., and Kaczmarek, L. K. (2005) *Soc. Neurosci. Abstr.* **846,** 2